Regulation of OPA1 processing and mitochondrial fusion by *m*-AAA protease isoenzymes and OMA1

Sarah Ehses,[1,2,3] Ines Raschke,[1,2,3] Giuseppe Mancuso,[5] Andrea Bernacchia,[5] Stefan Geimer,[7] Daniel Tondera,[8] Jean-Claude Martinou,[8] Benedikt Westermann,[7] Elena I. Rugarli,[5,6] and Thomas Langer[1,2,3,4]

[1]Institute for Genetics, [2]Centre for Molecular Medicine, and [3]Cologne Excellence Cluster on Cellular Stress Responses in Aging-Associated Diseases, University of Cologne, 50923 Cologne, Germany
[4]Max Planck Institute for the Biology of Aging, 50931 Cologne, Germany
[5]Laboratory of Genetic and Molecular Pathology, Neurological Institute Carlo Besta, 20133 Milano, Italy
[6]Department of Neuroscience and Medical Biotechnologies, University of Milano-Bicocca, 20052 Monza, Italy
[7]Electron Microscopy Laboratory, Institute for Cell Biology, University of Bayreuth, 95447 Bayreuth, Germany
[8]Department of Cell Biology, University of Geneva, 1211 Geneva 4, Switzerland

Mitochondrial fusion depends on the dynamin-like guanosine triphosphatase OPA1, whose activity is controlled by proteolytic cleavage. Dysfunction of mitochondria induces OPA1 processing and results in mitochondrial fragmentation, allowing the selective removal of damaged mitochondria. In this study, we demonstrate that two classes of metallopeptidases regulate OPA1 cleavage in the mitochondrial inner membrane: isoenzymes of the adenosine triphosphate (ATP)–dependent matrix AAA (ATPase associated with diverse cellular activities [*m*-AAA]) protease, variable assemblies of the conserved subunits paraplegin, AFG3L1 and -2, and the ATP-independent peptidase OMA1. Functionally redundant isoenzymes of the *m*-AAA protease ensure the balanced accumulation of long and short isoforms of OPA1 required for mitochondrial fusion. The loss of AFG3L2 in mouse tissues, down-regulation of AFG3L1 and -2 in mouse embryonic fibroblasts, or the expression of a dominant-negative AFG3L2 variant in human cells decreases the stability of long OPA1 isoforms and induces OPA1 processing by OMA1. Moreover, cleavage by OMA1 causes the accumulation of short OPA1 variants if mitochondrial DNA is depleted or mitochondrial activities are impaired. Our findings link distinct peptidases to constitutive and induced OPA1 processing and shed new light on the pathogenesis of neurodegenerative disorders associated with mutations in *m*-AAA protease subunits.

Introduction

Mitochondria are dynamic organelles that undergo continuous remodeling through fusion and fission events. Conserved protein machineries mediate fusion and fission of mitochondrial membranes (Cerveny et al., 2007; Hoppins et al., 2007; Westermann, 2008). The dynamin-related GTPase OPA1, which resides in the mitochondrial intermembrane space, is involved in inner membrane fusion, in the regulation of mitochondrial cristae morphology, and in protecting cells from apoptosis (Olichon et al., 2003; Griparic et al., 2004; Frezza et al., 2006; Meeusen et al., 2006; Lenaers et al., 2009). Mutations in OPA1 cause dominant optic atrophy, a progressive neurological disease characterized by degeneration of the retinal ganglion cells and atrophy of the optic nerve (Amati-Bonneau et al., 2009). Mitochondria contain various OPA1 isoforms that arise from alternative splicing and proteolytic processing events at two sites, S1 and S2, generating shorter isoforms (Delettre et al., 2001; Ishihara et al., 2006).

Correspondence to Elena I. Rugarli: Elena.Rugarli@uni-koeln.de; or Thomas Langer: Thomas.Langer@uni-koeln.de

E.I. Rugarli's present address is Biocenter, University of Cologne, 50674 Cologne, Germany.

Abbreviations used in this paper: AAA, ATPase associated with diverse cellular activities; CCCP, carbonyl cyanide *m*-chlorophenyl hydrazone; CHX, cycloheximide; *m*-AAA, matrix AAA; MEF, mouse embryonic fibroblast; mtDNA, mitochondrial DNA; *o*-phe, *o*-phenanthroline; PARL, presenilin-associated rhomboid-like protein; PS, proteolytic site; RCR, respiratory control ratio; SIMH, stress-induced mitochondrial hyperfusion; WB, Walker B; WT, wild type.

© 2009 Ehses et al. This article is distributed under the terms of an Attribution–Noncommercial–Share Alike–No Mirror Sites license for the first six months after the publication date (see http://www.jcb.org/misc/terms.shtml). After six months it is available under a Creative Commons License (Attribution–Noncommercial–Share Alike 3.0 Unported license, as described at http://creativecommons.org/licenses/by-nc-sa/3.0/).

The Rockefeller University Press $30.00
J. Cell Biol. Vol. 187 No. 7 1023–1036
www.jcb.org/cgi/doi/10.1083/jcb.200906084

THE JOURNAL OF CELL BIOLOGY

Downloaded from http://rupress.org/jcb/article-pdf/187/7/1023/1893434/jcb_200906084.pdf by guest on 23 April 2024

A combination of long and short OPA1 isoforms is required for mitochondrial fusion (Song et al., 2007), pointing to a crucial regulatory role of OPA1 processing. Roughly equimolar concentrations of long and short isoforms of OPA1 are formed under normal conditions. However, low mitochondrial ATP levels, the dissipation of the membrane potential across the inner membrane ($\Delta\psi_m$), or apoptotic stimuli induce OPA1 cleavage, resulting in the loss of long isoforms (Duvezin-Caubet et al., 2006; Ishihara et al., 2006; Baricault et al., 2007). Various proteases in the inner membrane have been linked to the processing of OPA1. The intermembrane space AAA (ATPase associated with diverse cellular activities) protease YME1L1 regulates OPA1 cleavage at S2, which is only present in a subset of OPA1 variants (Griparic et al., 2007; Song et al., 2007). Debate exists about the protease cleaving OPA1 at S1, as both the rhomboid protease PARL (presenilin-associated rhomboid-like protein) and the matrix AAA (*m*-AAA) protease, an oligomeric ATP-dependent metallopeptidase in the inner membrane, have been proposed to be involved in OPA1 processing (Cipolat et al., 2006; Ishihara et al., 2006). However, normal OPA1 processing in mouse embryonic fibroblasts (MEFs) lacking PARL or the *m*-AAA protease subunit paraplegin raised doubts about the role of either protease for OPA1 processing in vivo (Duvezin-Caubet et al., 2007).

Notably, human and murine mitochondria possess different *m*-AAA protease isoenzymes, which differ in their subunit composition but exert at least partially redundant activities (Koppen et al., 2007). Three homologous subunits are expressed in the mouse, AFG3L1 and -2 and paraplegin. Whereas paraplegin was exclusively detected in heterooligomeric complexes with AFG3L1 and -2, homooligomeric complexes composed of AFG3L1 or -2 do exist. Therefore, functionally redundant isoenzymes might substitute for the loss of paraplegin and maintain OPA1 processing in the absence of paraplegin. A complementation study in yeast indeed demonstrated functional conservation of different mammalian *m*-AAA protease isoenzymes and revealed their ability to cleave OPA1 expressed heterologously in yeast (Duvezin-Caubet et al., 2007). This notwithstanding, they have been linked to different neurodegenerative diseases in human: mutations in *Spg7* encoding paraplegin cause a recessive form of hereditary spastic paraplegia, whereas heterozygous mutations in *Afg3l2* are responsible for a dominant form of spinocerebellar ataxia, SCA28 (Cagnoli et al. 2008. Annual meeting of the American Society of Human Genetics. Abstr. 1501; DiBella et al. 2008. Annual meeting of the American Society of Human Genetics. Abstr. 216). It is presently unclear whether this reflects functional differences of *m*-AAA isoenzymes or results from a tissue-specific expression of *m*-AAA protease subunits (Koppen et al., 2007).

In this study, we have assessed the function of different *m*-AAA isoenzymes in vivo using RNAi and demonstrate that OPA1 processing and mitochondrial fusion depend on AFG3L1 and -2. Moreover, we identify a novel peptidase in the inner membrane, OMA1, which mediates OPA1 processing if *m*-AAA proteases are absent or mitochondrial activities are impaired.

Results

AFG3L1 and -2 are required for mitochondrial fusion

We used RNAi in MEFs to down-regulate *m*-AAA protease subunits individually or in combination. Immunoblotting revealed effective depletion of AFG3L1 and -2 and paraplegin (Fig. 1 A). Mitochondrial morphology was monitored by fluorescence microscopy in cells cotransfected with a mitochondrially targeted DsRed variant. Neither paraplegin-depleted mitochondria nor mitochondria from *Spg7*$^{-/-}$ MEFs showed morphological abnormalities (Fig. S1 and not depicted). Similarly, mitochondria of cells transfected with either *Afg3l1*- or *Afg3l2*-specific siRNA appeared largely normal in morphology (Fig. 1, B and C). However, concomitant down-regulation of both subunits caused fragmentation of the mitochondrial network in ~80% of the cells (Fig. 1, B and C). Examination of these cells by electron microscopy revealed a severe disturbance of the mitochondrial ultrastructure (Fig. 1 D). Lamellar cristae were either completely absent or severely reduced in number in cells lacking AFG3L1 and -2, whereas the structure of cristae was not significantly affected upon down-regulation of AFG3L1 or -2 (Fig. 1 D). These findings reveal overlapping activities of AFG3L1 and -2 and demonstrate an essential role of the *m*-AAA protease for the ultrastructure of mitochondria.

An impaired fusion or increased fission may cause fragmentation of the mitochondrial network in the absence of AFG3L1 and -2. To distinguish between these possibilities, we transfected interfered cells with a dominant-negative variant of the fission component DRP1, DRP1^{K38A}. In agreement with previous observations (Smirnova et al., 1998; James et al., 2003), expression of DRP1^{K38A} impaired fission and resulted in the elongation of mitochondrial tubules as the result of ongoing fusion (Fig. 2, A and B). In contrast, cells lacking AFG3L1 and -2 maintained punctiform mitochondria upon expression of DRP1^{K38A}, strongly suggesting that the organelles are unable to fuse. As independent evidence, we found that cells interfered for *Afg3l2* and *-1* did not form a highly interconnected network when exposed to low concentrations of cycloheximide (CHX; Fig. 2, C and D), indicating that they have lost the ability to undergo stress-induced mitochondrial hyperfusion (SIMH), which is an adaptive response against stress (Tondera et al., 2009). Therefore, we conclude that the fusion of mitochondrial membranes depends on AFG3L1 and -2.

The *m*-AAA protease controls the stability of L-OPA1

OPA1 regulates both mitochondrial fusion and cristae morphogenesis (Lenaers et al., 2009). MEFs express mainly two alternative transcripts of OPA1, variants 1 and 7, which are cleaved, resulting in the accumulation of five OPA1 forms: two long (a and b) and three short isoforms (c–e; Ishihara et al., 2006; Duvezin-Caubet et al., 2007). Down-regulation of individual subunits of the *m*-AAA protease isoenzymes did not reproducibly affect the processing of OPA1 (Fig. 3 A). However, the concomitant loss of AFG3L1 and -2 significantly affected the accumulation of OPA1 variants (Fig. 3 A): the

Downloaded from http://rupress.org/jcb/article-pdf/187/7/1023/1893434/jcb_200906084.pdf by guest on 23 April 2024

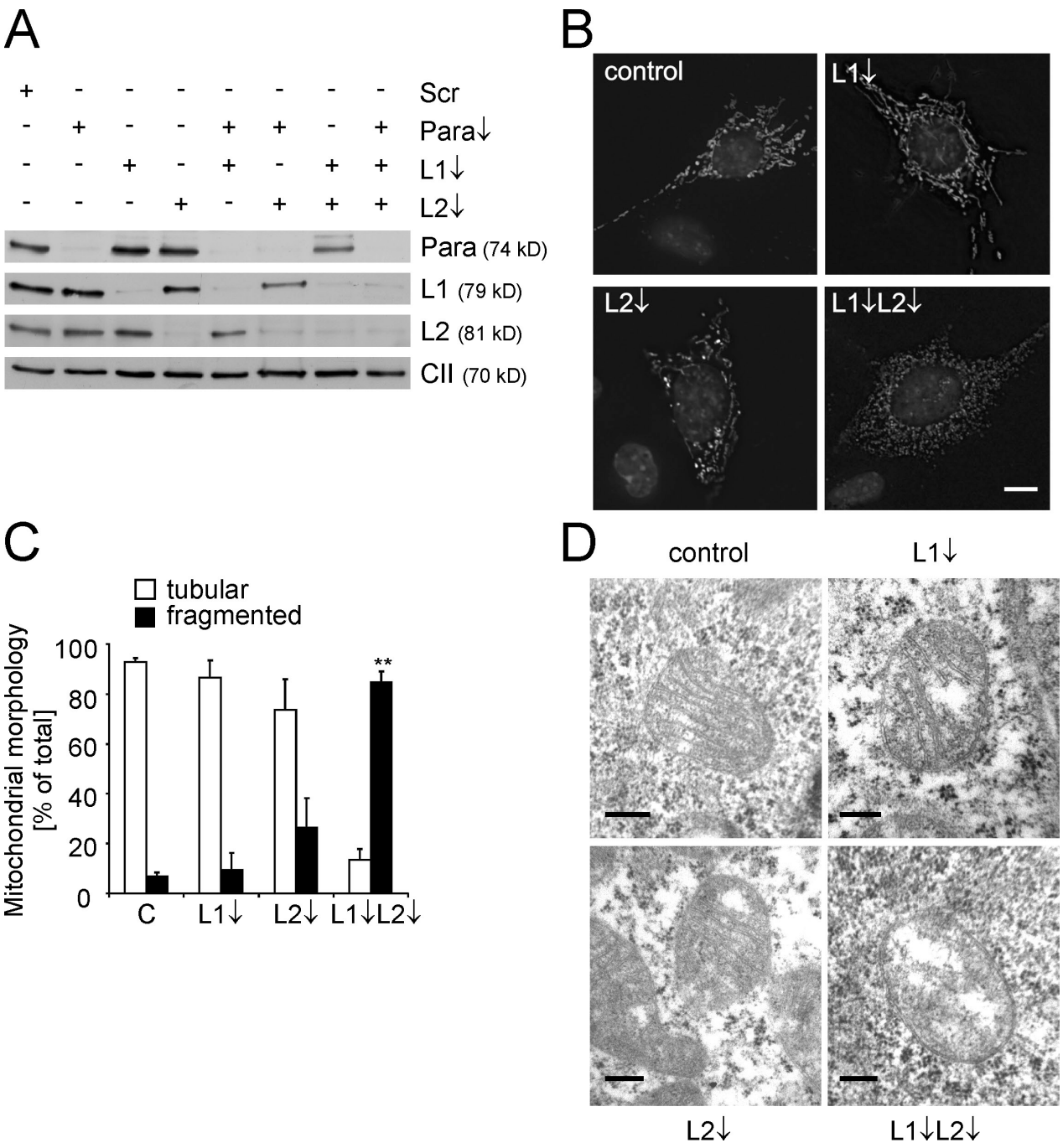

Figure 1. **Fragmentation of mitochondria in MEFs depleted of AFG3L1 and -2.** (A) Immunoblot analysis of MEFs transfected with siRNAs directed against AFG3L1 and -2 and paraplegin or scrambled siRNA (Scr) using specific antisera recognizing paraplegin (Para), AFG3L1 (L1), AFG3L2 (L2), and the 70-kD subunit of complex II (CII). (B and C) Mitochondrial morphology in AFG3L1- and AFG3L2-deficient MEFs was visualized by expression of mito-DsRed, and nuclear DNA was stained with DAPI. >150 MEFs were scored in each experiment. Bars represent means ± SD of three independent experiments (**, $P < 0.01$). (D) Mitochondrial ultrastructure in MEFs transfected with scrambled or AFG3L1- or AFG3L2-specific siRNAs or siRNAs against AFG3L1 and -2. Representative transmission electron micrographs of mitochondria are shown. Bars: (B) 10 µm; (D) 0.2 µm.

long OPA1 isoforms were no longer detected, whereas short forms, mainly e, accumulated (Fig. 3 A). This shift was not significantly enhanced in *Spg7*$^{-/-}$ cells (Fig. 3 A). These results substantiate the overlapping activities of AFG3L1 and -2 and point to an impaired OPA1 processing in *m*-AAA protease–depleted MEFs.

Both long and short OPA1 isoforms are necessary to support mitochondrial fusion (Song et al., 2007). Therefore, the loss of long OPA1 isoforms can account for the fragmentation of the mitochondrial network upon depletion of AFG3L1 and -2. To test this hypothesis, we assessed mitochondrial morphology after coexpression of *Afg3l1* and *-2* siRNAs with a Flag-tagged version of OPA1 splicing variant 1 (v1), in which the amino acid residues flanking the processing site had been deleted (v1ΔS1; Ishihara et al., 2006). Mitochondrial morphology was also analyzed in AFG3L1- and

Downloaded from http://rupress.org/jcb/article-pdf/187/7/1023/1893434/jcb_200906084.pdf by guest on 23 April 2024

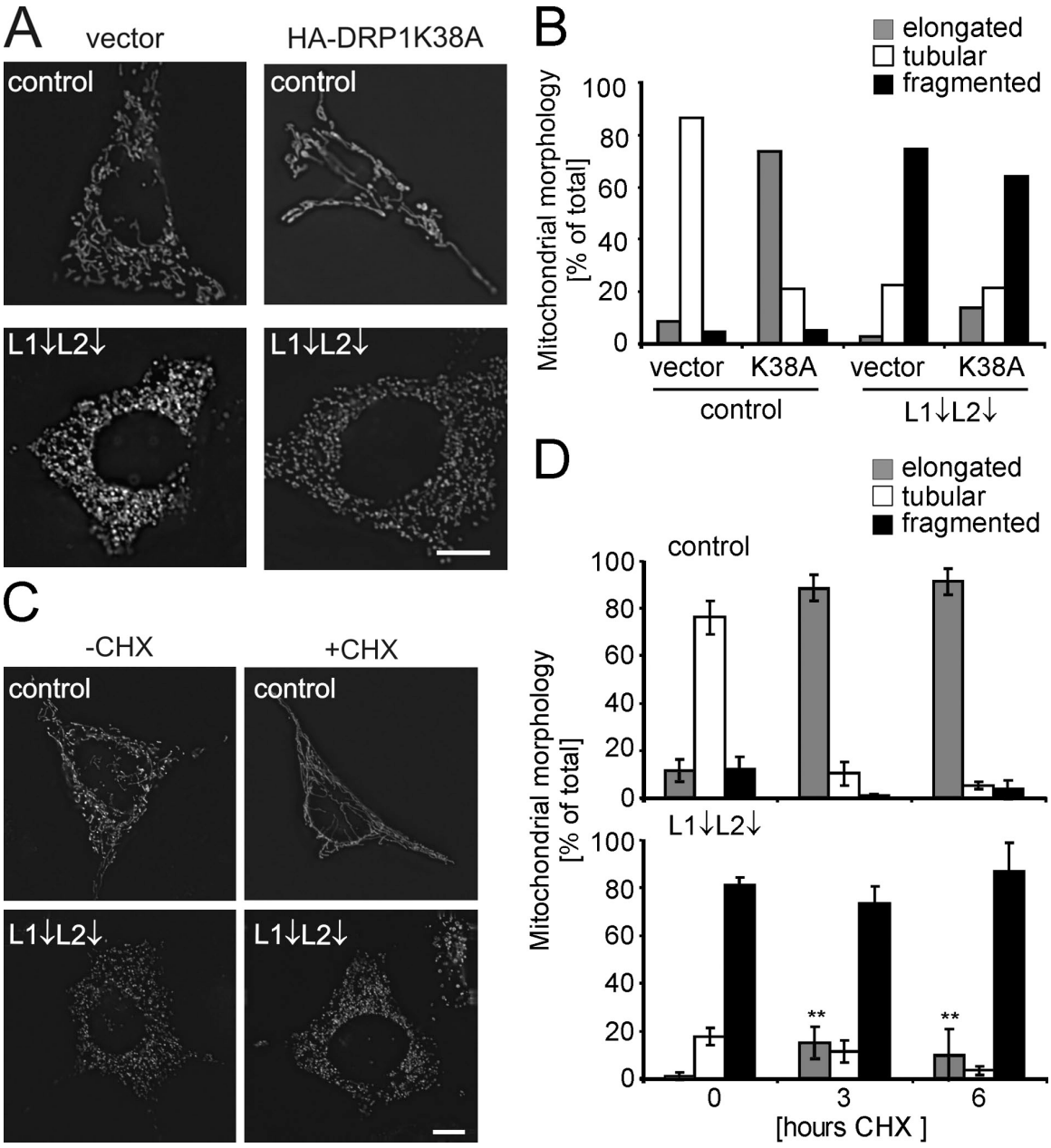

Figure 2. **AFG3L1 and -2 are required for mitochondrial fusion.** (A and B) Inhibition of fission does not restore a tubular network in the absence of AFG3L1 (L1) and AFG3L2 (L2). Dominant-negative DRP1^{K38A}-HA and mito-DsRed were expressed in *m*-AAA protease–deficient MEFs, and mitochondrial morphology was assessed after 24 h. >200 cells were scored per experiment. (C and D) SIMH depends on AFG3L1 and -2. After depletion of AFG3L1 and -2, MEFs were incubated for 3 (C and D) and 6 h (D) in the presence of 1 µM CHX (+CHX) as indicated. >150 cells were scored for each experiment. Bars represent means ± SD of three independent experiments (**, $P < 0.01$). Bars, 10 µm.

AFG3L2-depleted MEFs expressing S-OPA1, a hybrid protein composed of a short form of OPA1 fused to the mitochondrial target sequence of apoptosis-inducing factor (Ishihara et al., 2006). We observed a partial but statistically significant restoration of a tubular network in *m*-AAA protease–deficient cells upon expression of v1ΔS1 but not of S-OPA1 (Fig. 3 B), suggesting that the *m*-AAA protease regulates mitochondrial fusion via OPA1.

These findings link, for the first time, the function of AFG3L1 and -2 to the biogenesis of OPA1. Surprisingly, depletion of AFG3L1 and -2 caused a loss rather than a stabilization of long OPA1 isoforms. Therefore, we directly monitored the efficiency of OPA1 processing in the absence of *m*-AAA protease subunits by expressing Flag-tagged v1 or v1ΔS1 in MEFs (Ishihara et al., 2006). Down-regulation of AFG3L1 and -2 promoted processing of v1 and led to the loss of long OPA1 forms (Fig. 3 C). v1ΔS1 was present at severely decreased levels in cells lacking both *m*-AAA protease subunits, suggesting degradation of the OPA1 variant (Fig. 3 C). Indeed, if protein synthesis was inhibited by CHX, v1ΔS1 was stable upon further incubation of control cells (Fig. 3 D). In contrast, v1ΔS1 level decreased in the absence of AFG3L1 and -2 (Fig. 3 D), explaining the only

Downloaded from http://rupress.org/jcb/article-pdf/187/7/1023/1893434/jcb_200906084.pdf by guest on 23 April 2024

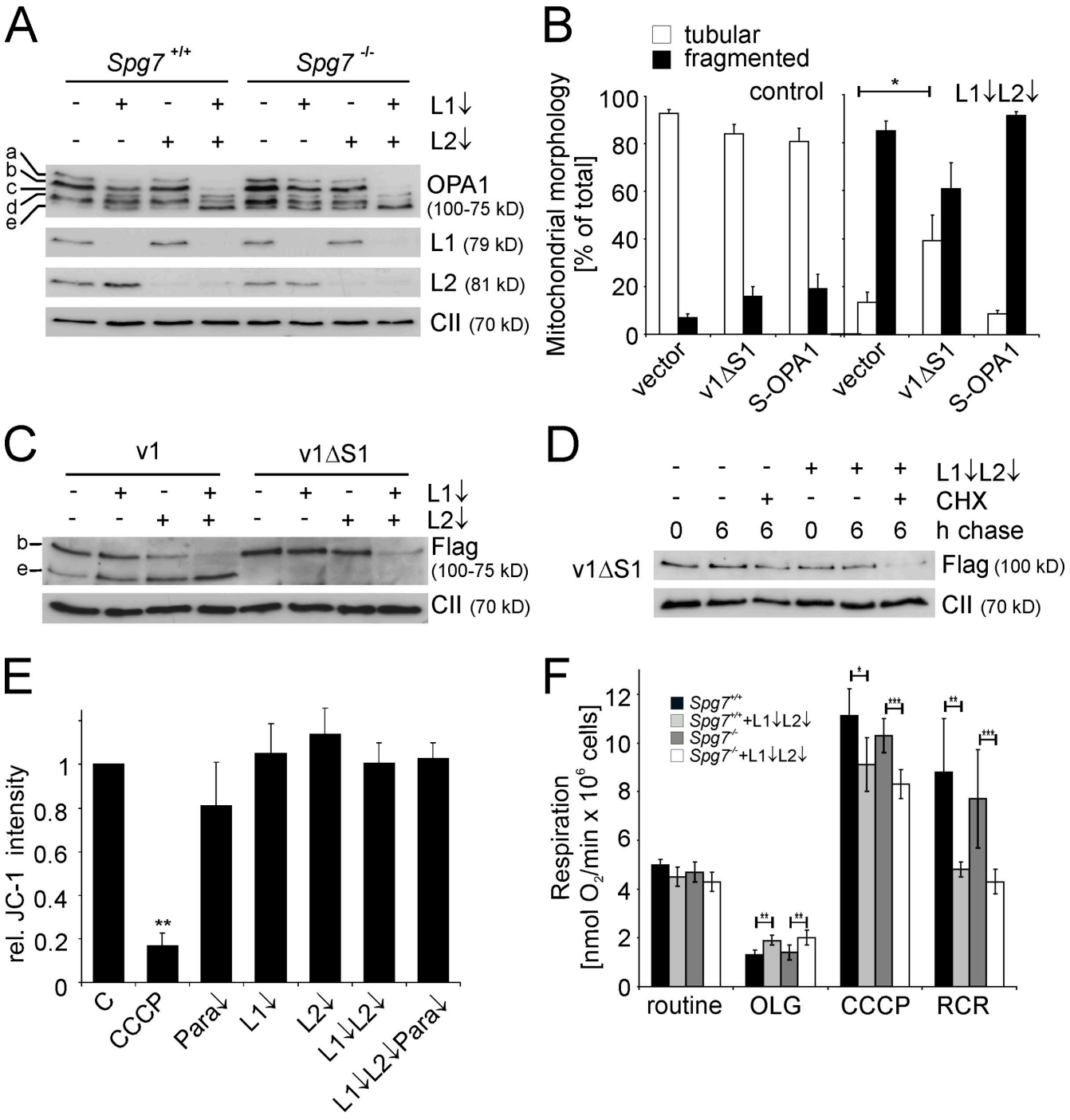

Figure 3. **Destabilization of long OPA1 isoforms in the absence of the *m*-AAA protease.** (A) Immunoblot analysis of *Spg7*$^{+/+}$ and *Spg7*$^{-/-}$ MEFs depleted of AFG3L1 (L1) and AFG3L2 (L2) as indicated. Cells lysates were analyzed with antibodies directed against OPA1, AFG3L1 and -2 and, for control, the 70-kD subunit of complex II (CII). OPA1 isoforms are marked with a–e. (B) Mitochondrial morphology in AFG3L1/AFG3L2-deficient MEFs expressing OPA1 variants. Before depletion of AFG3L1 and -2, MEFs were transfected with plasmids encoding Flag-tagged OPA1 variants v1ΔS1 or S-OPA1. >150 cells were scored. Bars represent means ± SD of three independent experiments (*, $P < 0.05$). (C) Immunoblot analysis of AFG3L1/AFG3L2-deficient MEFs expressing Flag-tagged OPA1 splice variants 1 (v1) and 1ΔS1 (v1ΔS1). Cell lysates were analyzed 3 d after siRNA transfection by SDS-PAGE and immunoblotting using anti-Flag and anti–complex II antibodies. (D) Degradation of v1ΔS1 in AFG3L1/AFG3L2-depleted MEFs. 2 d after siRNA transfection, cells were incubated for 6 h with 100 µg/ml CHX and analyzed as described in C. (E) Mitochondrial membrane potential in MEFs depleted of *m*-AAA protease subunits was analyzed with the fluorescent dye JC-1 and flow cytometry at 590 nm. Dissipation of the membrane potential with CCCP was used as a control. Relative intensities to cells transfected with scrambled RNAi (C) are shown. Data represent means ± SD of three independent experiments (**, $P < 0.01$). Para, paraplegin. (F) Oxygen consumption in *Spg7*$^{+/+}$ and *Spg7*$^{-/-}$ MEFs depleted of AFG3L1/AFG3L2 was measured under routine conditions and in the presence of oligomycin (OLG) and CCCP. Bars represent means ± SD of three independent experiments (*, $P < 0.05$; **, $P < 0.01$; ***, $P < 0.001$).

Downloaded from http://rupress.org/jcb/article-pdf/187/7/1023/1893434/jcb_200906084.pdf by guest on 23 April 2024

partial restoration of the tubular mitochondrial network upon expression of this variant in AFG3L1/AFG3L2-depleted cells (Fig. 3 B). We conclude from these experiments that turnover, as well as cleavage, of OPA1 at S1 is enhanced upon down-regulation of *m*-AAA protease subunits.

Respiratory activity of *m*-AAA protease–deficient mitochondria

Disruption of the mitochondrial membrane potential and decreased ATP levels within mitochondria have been shown to induce processing of OPA1 (Duvezin-Caubet et al., 2006; Baricault et al., 2007). Respiratory chain deficiencies have recently been reported in brain mitochondria of *Afg3l2*$^{-/-}$ mice (Maltecca et al., 2008). Therefore, we assessed the formation of the mitochondrial membrane potential in cells depleted of *m*-AAA protease subunits using the membrane potential–dependent fluorescent dye JC-1 (Fig. 3 E). Whereas fluorescence dropped upon dissipation of the membrane potential by carbonyl cyanide *m*-chlorophenyl hydrazone (CCCP), the membrane potential was maintained upon depletion of *m*-AAA protease subunits (Fig. 3 E). Similarly, TMRE (tetramethylrhodamine, ethyl ester) measurements in *Afg3l2*$^{-/-}$ MEFs grown on glucose or galactose did not reveal an impaired membrane potential (Fig. S2).

In subsequent experiments, we measured oxygen consumption in MEFs lacking *m*-AAA protease subunits to evaluate phosphorylating respiration with endogenous substrates. Down-regulation of AFG3L1 and -2 did not significantly affect oxygen consumption, irrespective of the presence of paraplegin (Fig. 3 F). However, respiration was significantly increased upon inhibition of the mitochondrial F_1F_O-ATP synthase with oligomycin, suggesting a higher proton leakage under conditions of membrane hyperpolarization (Fig. 3 F). In *m*-AAA protease–depleted cells, we also observed a small but significant decrease of the maximum respiratory capacity, which was measured under uncoupled conditions (Fig. 3 F). Accordingly, the ratio of uncoupled respiration and oligomycin-inhibited respiration, which is the respiratory control ratio (RCR), was reduced to ~50% when AFG3L1 and -2 were down-regulated (Fig. 3 F). The loss of paraplegin did not further decrease the RCR (Fig. 3 F). These results indicate that the capacity of the oxidative phosphorylation system to supply ATP under conditions of high energy demand is limited in the absence of the *m*-AAA protease. However, under normal conditions, respiration was not impaired upon down-regulation of *m*-AAA protease subunits, suggesting that AFG3L1 and -2 directly affect mitochondrial fusion.

A dominant-negative mutant of AFG3L2

To substantiate the role of the *m*-AAA protease for OPA1 processing, we generated mutant variants of AFG3L2, in which glutamate 408 within the Walker B (WB) motif of the AAA domain or glutamate 575 within the proteolytic site (PS) were replaced by glutamine (WB, E408Q; PS, E575Q). Although glutamate 575 is essential for proteolytic activity, glutamate 408 is conserved within AAA+ ATPases and is required to activate a water molecule for nucleophilic attack on bound ATP. AAA+ ATPases harboring a corresponding mutation in the WB motif lack ATPase activity and trap ATP (Weibezahn et al., 2003; Dalal et al., 2004; Augustin et al., 2009). We established stable HEK293 cell lines allowing the tetracycline-inducible expression of C-terminally tagged AFG3L2 variants. In contrast to mouse fibroblasts, human cells express only two *m*-AAA protease subunits, AFG3L2 and paraplegin (Kremmidiotis et al., 2001). Induction of AFG3L2 expression in the presence of tetracycline resulted in an approximately twofold overexpression of AFG3L2 (Fig. 4 B). Although overexpression of AFG3L2 or AFG3L2^{E575Q} (PS) did not affect cell growth, cells expressing AFG3L2^{E408Q} (WB) showed a prominent reduction of their growth rate (Fig. 4 A), indicating that AFG3L2^{E408Q} (WB) but not AFG3L2^{E575Q} (PS) exerts a dominant-negative effect on other *m*-AAA protease subunits.

Long OPA1 isoforms were destabilized in the presence of AFG3L2^{E408Q} (WB), although they accumulated at normal levels upon expression of AFG3L2 or AFG3L2^{E575Q} (PS) (Fig. 4 B). Consistently, the analysis of mitochondrial morphology in these cell lines revealed fragmentation of the mitochondrial network in the majority of cells expressing AFG3L2^{E408Q} (WB) (Fig. 4, C and D). In contrast, expression of AFG3L2 of AFG3L2^{E575Q} (PS) did not affect the morphology of mitochondria (Fig. 4, C and D). Expression of the dominant-negative AFG3L2 variant did not dissipate the mitochondrial membrane potential in HEK293 cells (Fig. 4 E), nor was the oxygen consumption of HEK293 cells impaired (Fig. 4 F). However, similar to *m*-AAA protease–deficient MEFs, we observed a reduced RCR in cells expressing AFG3L2^{E408Q} (WB) (Fig. 4 F), suggesting an impaired energy metabolism under conditions of high energy demand. We conclude from these experiments that expression of a dominant-negative variant of AFG3L2 and depletion of *m*-AAA protease subunits by RNAi similarly affect mitochondrial morphology and OPA1 processing.

OMA1 mediates OPA1 processing in the absence of *m*-AAA proteases

Our results suggest that an unidentified protease mediates processing and degradation of the long OPA1 isoforms in *m*-AAA protease–deficient cells. Notably, lack of paraplegin (Fig. 3 A), PARL, or HtrA2/Omi did not stabilize L-OPA1 in the absence of AFG3L1 and -2 (Fig. S3 A). Furthermore, concomitant down-regulation of AFG3L1 and -2 with YME1L1 or LON did not rescue long OPA1 isoforms (Fig. S3 B). To restrict the number of possible proteases involved in this process, we incubated AFG3L1/AFG3L2-deficient MEFs expressing v1 with different protease inhibitors and monitored the accumulation of Flag-tagged v1 and endogenous OPA1 by immunoblotting (Fig. 5 A). The stability of OPA1 was not affected upon incubating cells with pepstatin A, E-64d, or the broad-spectrum serine protease inhibitor Pefabloc (Fig. 5 A). In contrast, *o*-phenanthroline (*o*-phe), a membrane-permeable metalloprotease inhibitor, stabilized v1, resulting in the accumulation of the long as well as the precursor form of OPA1 (Fig. 5 A). This is consistent with previous experiments on CCCP-induced OPA1 processing (Ishihara et al., 2006). Similarly, the proteasome inhibitor MG132 stabilized v1 in AFG3L1/AFG3L2-depleted cells (Fig. 5 A). Thus, OPA1 levels in mitochondria depend critically on the activity of

Downloaded from http://rupress.org/jcb/article-pdf/187/7/1023/1893434/jcb_200906084.pdf by guest on 23 April 2024

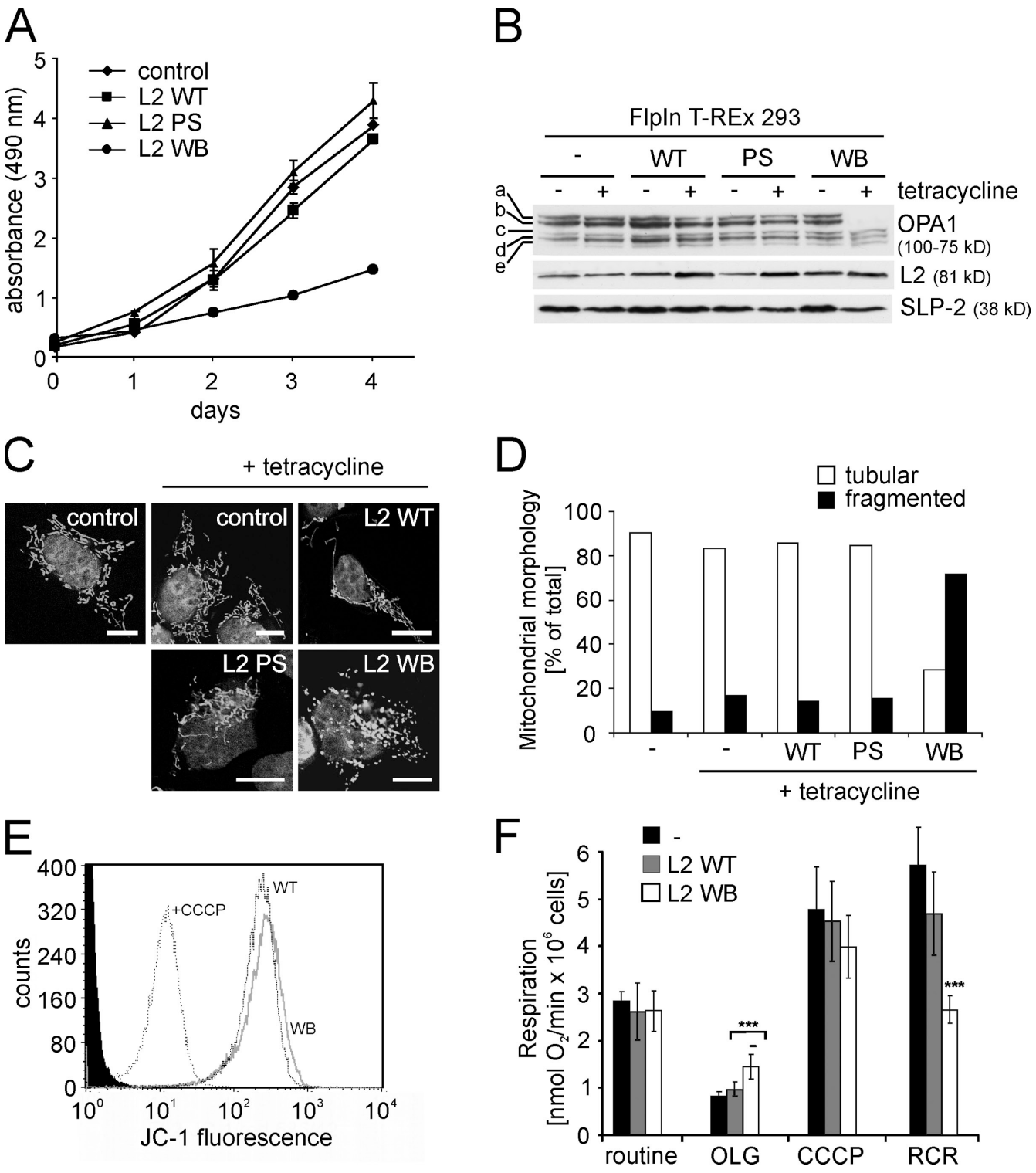

Figure 4. **Expression of dominant-negative AFG3L2^{E408Q} inhibits cell proliferation and impairs mitochondrial morphology and OPA1 processing.** (A) Growth of cells expressing AFG3L2 (L2 WT), AFG3L2^{E575Q} (L2 PS), or AFG3L2^{E408Q} (L2 WB). Graphs represent means ± SD of three independent experiments. (B) Immunoblot analysis of FlpIn T-REx 293 cells expressing AFG3L2 variants. Cell lysates were analyzed 24 h after the addition of tetracycline using antibodies directed against OPA1, AFG3L2, and SLP-2. (C and D) Mitochondrial morphology in cells expressing AFG3L2 variants. >100 cells were scored. WT, AFG3L2; PS, AFG3L2^{E575Q}; WB, AFG3L2^{E408Q}. (E) Membrane potential in cells expressing AFG3L2 (WT) or AFG3L2^{E408Q} (WB). (F) Oxygen consumption in cells expressing AFG3L2 (WT) or AFG3L2^{E408Q} (WB) measured as in Fig. 3 F. Error bars represent the means ± SD of a minimum of three independent experiments (***, $P < 0.001$). Bars, 10 µm.

Downloaded from http://rupress.org/jcb/article-pdf/187/7/1023/1893434/jcb_200906084.pdf by guest on 23 April 2024

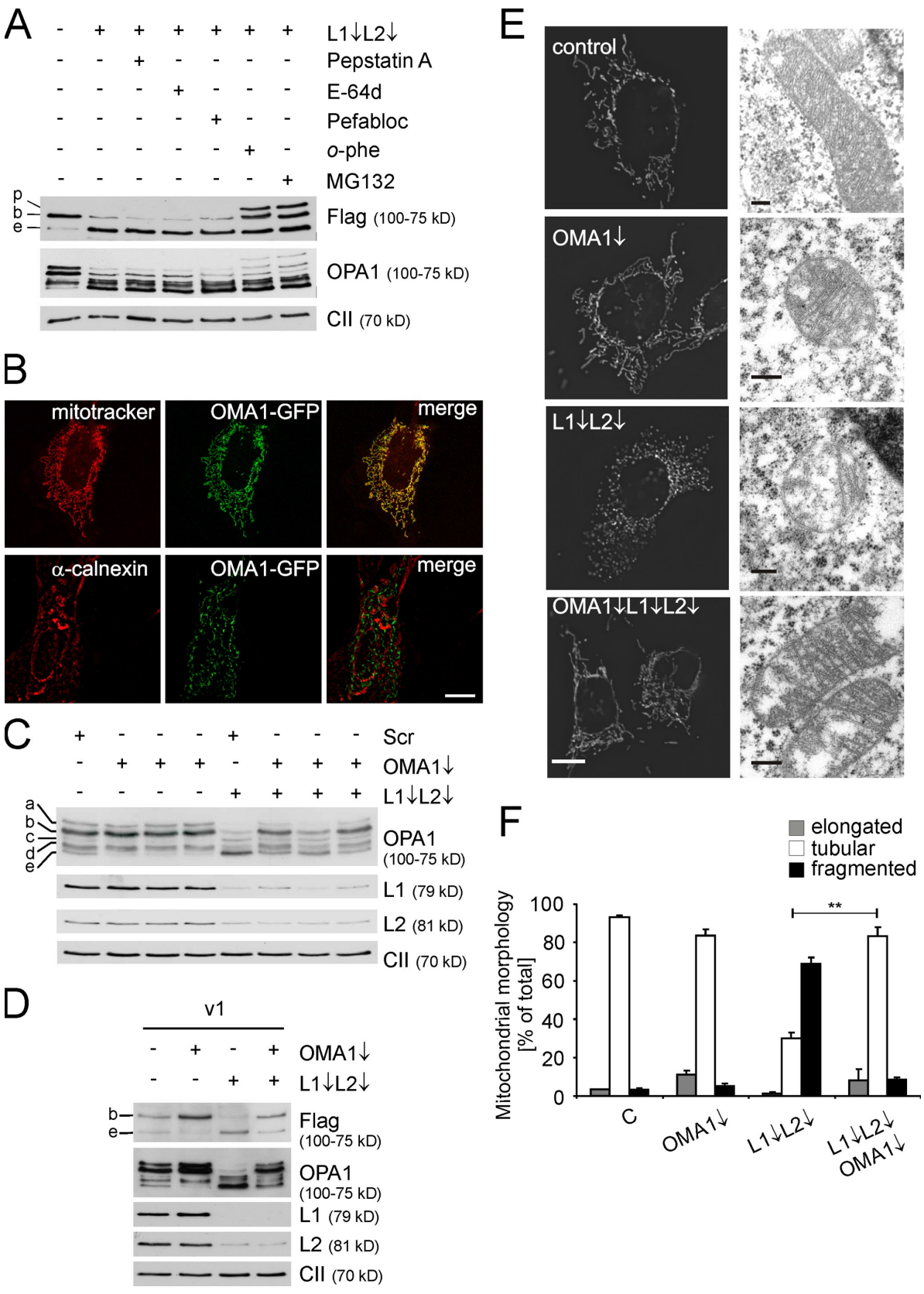

Figure 5. **OMA1 degrades OPA1 in AFG3L1/AFG3L2-deficient MEFs.** (A) Stability of OPA1 and OPA1 variant 1 in the presence of different protease inhibitors. Flag-tagged OPA1 variant 1 was expressed in MEFs that were subsequently depleted of AFG3L1 (L1) and AFG3L2 (L2). After 48 h, MEFs were incubated for 5 h with pepstatin A, E-64d, Pefabloc SC, *o*-phe, or MG132, and cell lysates were analyzed by immunoblotting with α-Flag, α-OPA1, and α–complex II. p, OPA1 precursor; b, long OPA1 isoform; e, short OPA1 isoform. (B) Localization of OMA1 to mitochondria. Fluorescence microscopy of MEFs expressing murine OMA1 harboring a C-terminal GFP tag. Mitochondria were stained with MitoTracker red CMXRos, whereas the ER was detected

Downloaded from http://rupress.org/jcb/article-pdf/187/7/1023/1893434/jcb_200906084.pdf by guest on 23 April 2024

26-S proteasomes and an unknown metallopeptidase. It is conceivable that inhibition of the general mitochondrial processing peptidase causes the accumulation of the precursor form of OPA1 within mitochondria in the presence of *o*-phe. Similarly, 26-S proteasomes may degrade newly synthesized OPA1 in the cytosol before import into mitochondria rather than mediating the turnover of preexisting mitochondrial OPA1. In agreement with this hypothesis, MG132 did not stabilize v1ΔS1 in the absence of AFG3L1 and -2 when cytosolic protein synthesis was inhibited by CHX (Fig. S3 C). Thus, the inhibitor experiments did not allow us to identify proteases controlling the stability of L-OPA1 within mitochondria.

We have previously identified Oma1 in the inner membrane of yeast mitochondria as a metallopeptidase, whose activity overlaps with the *m*-AAA protease (Oma1 for overlapping activity with *m*-AAA protease 1; Käser et al., 2003). Oma1 is conserved in evolution with homologous proteases present in vertebrates. However, human OMA1 has been localized to the ER membrane (Bao et al., 2003). To reexamine the subcellular localization of OMA1, we expressed an OMA1 variant harboring a C-terminal GFP domain in MEFs (Fig. 5 B). OMA1-GFP was exclusively localized to mitochondria and not detected in the ER membrane (Fig. 5 B). Similarly, a tubular mitochondrial network was visible in immunofluorescence experiments after transient expression of an OMA1 variant harboring a C-terminal Flag tag (unpublished data). We conclude that OMA1, as yeast Oma1, is localized in mitochondria.

To examine whether OMA1 affects OPA1 processing in the mitochondrial inner membrane, we used three different oligonucleotides directed against *Oma1* for RNAi. Quantitative RT-PCR experiments revealed efficient down-regulation of *Oma1* transcripts by >80% (Fig. S4 A). Depletion of OMA1 slightly reduced the level of OPA1 isoforms c and e, which are generated by S1 cleavage and accumulate at low levels under these conditions in MEFs (Fig. 5 C). However, we observed a significant stabilization of L-OPA1 in AFG3L1/AFG3L2-deficient MEFs upon down-regulation of OMA1, whereas transfection of the cells with scrambled oligonucleotides had no effect (Fig. 5 C).

We monitored OPA1 processing directly after transient expression of the Flag-tagged OPA1 variant v1 in MEFs (Fig. 5 D). In the presence of AFG3L1 and -2, Flag-tagged L-OPA1 accumulated in OMA1-depleted cells (Fig. 5 D), indicating that OMA1 is able to cleave overexpressed OPA1. In contrast, in the absence of AFG3L1 and -2, down-regulation of OMA1 stabilized L-OPA1, demonstrating that OMA1 mediates turnover and increased OPA1 processing in the absence of the *m*-AAA protease (Fig. 5 D).

OPA1 isoforms accumulated virtually as in wild-type (WT) cells in MEFs depleted of both OMA1 and the *m*-AAA protease. Therefore, we examined the morphology of the mitochondrial network after expression of a mitochondrially targeted DsRed variant in these cells (Fig. 5, E and F). Depletion of OMA1 did not significantly affect mitochondrial morphology in the presence of the *m*-AAA protease but restored the tubular network in AFG3L1/AFG3L2-deficient MEFs (Fig. 5, E and F). Electron micrographs revealed a normal, lamellar cristae morphology of mitochondria lacking both the *m*-AAA protease and OMA1 (Fig. 5 E). These findings substantiate our conclusion that the *m*-AAA protease regulates mitochondrial fusion via OPA1 and demonstrate that OMA1 is epistatic to the *m*-AAA protease.

To further define the functional interrelationship of OMA1 and the *m*-AAA protease, we assessed the assembly of *m*-AAA proteases in OMA1-depleted mitochondria by blue-native gel electrophoresis (Fig. S4 B). Down-regulation of OMA1 did not affect the formation of the proteolytic complexes containing AFG3L2 and/or -1. Moreover, depletion of OMA1 did not interfere with the maturation of AFG3L1 or -2 (Fig. 5 C and Fig. S5), which occurs autocatalytically upon import into mitochondria (Koppen et al., 2009). Similarly, processing of an OMA1 variant carrying a C-terminal myc tag was not impaired in mitochondria depleted of AFG3L1 and -2 (Fig. S4 C).

Tissue-specific destabilization of L-OPA1 in *Afg3l2*$^{-/-}$ mice

Mutations in the *m*-AAA protease subunits paraplegin and AFG3L2 cause neurodegeneration in human, but molecular details of the pathogenesis are currently not understood. Our experiments revealed an at least partially redundant function of AFG3L1 and -2 for mitochondrial fusion in MEFs (Fig. 1). However, as AFG3L1 is a pseudogene in humans (Kremmidiotis et al., 2001) and is expressed at low levels in the mouse brain (Koppen et al., 2007; Martinelli et al., 2009), it is conceivable that the regulation of OPA1 processing by the *m*-AAA protease is of potential pathogenic relevance. To examine whether the loss of AFG3L2 impairs OPA1 cleavage in vivo, we monitored OPA1 processing in mitochondria isolated from tissues of a recently established *Afg3l2*$^{-/-}$ mouse line (Maltecca et al., 2008). The abundance of individual OPA1 isoforms varies in different tissues, as previously described (Fig. 6 A; Akepati et al., 2008). In the absence of AFG3L2, L-OPA1 isoforms accumulated at strongly reduced levels in the brain, heart, and kidney, demonstrating that the stability of L-OPA1 depends on AFG3L2 in vivo. Notably, deletion of *Afg3l2* hardly affected OPA1 isoforms in the liver (Fig. 6 A), which is consistent with a compensatory effect of AFG3L1, which is expressed at higher levels relative to AFG3L2 in the liver (Koppen et al., 2007).

To analyze whether depletion of OMA1 can suppress deleterious effects of the loss of the *Afg3l2* gene, we monitored OPA1

using an antiserum directed against calnexin. (C) Immunoblot analysis of MEFs transfected with siRNAs directed against AFG3L1 and -2 and OMA1 or scrambled siRNA (Scr) using specific antisera recognizing OPA1, AFG3L1 and -2, and the 70-kD subunit of complex II (CII). Three different siRNAs directed against OMA1 were used. (D) Immunoblot analysis of MEFs transfected with siRNAs directed against AFG3L1/AFG3L2 and OMA1 and Flag-tagged OPA1 splice variant 1 (v1). Cell lysates were analyzed 3 d after transfection by SDS-PAGE and immunoblotting using α-Flag, α-AFG3L1, α-AFG3L2, α-OPA1, and α–complex II antibodies. (E) Mitochondrial morphology in MEFs transfected with AFG3L1/AFG3L2 and OMA1 siRNA was visualized by expression of mito-DsRed (left). Mitochondrial ultrastructure was analyzed by electron microscopy. (F) Quantification of mitochondrial morphology. >150 MEFs were scored in each immunofluorescence experiment. Bars represent means ± SD of three independent experiments (**, $P < 0.01$). Bars: (B) 10 µm; (E) 0.2 µm.

Downloaded from http://rupress.org/jcb/article-pdf/187/7/1023/1893434/jcb_200906084.pdf by guest on 23 April 2024

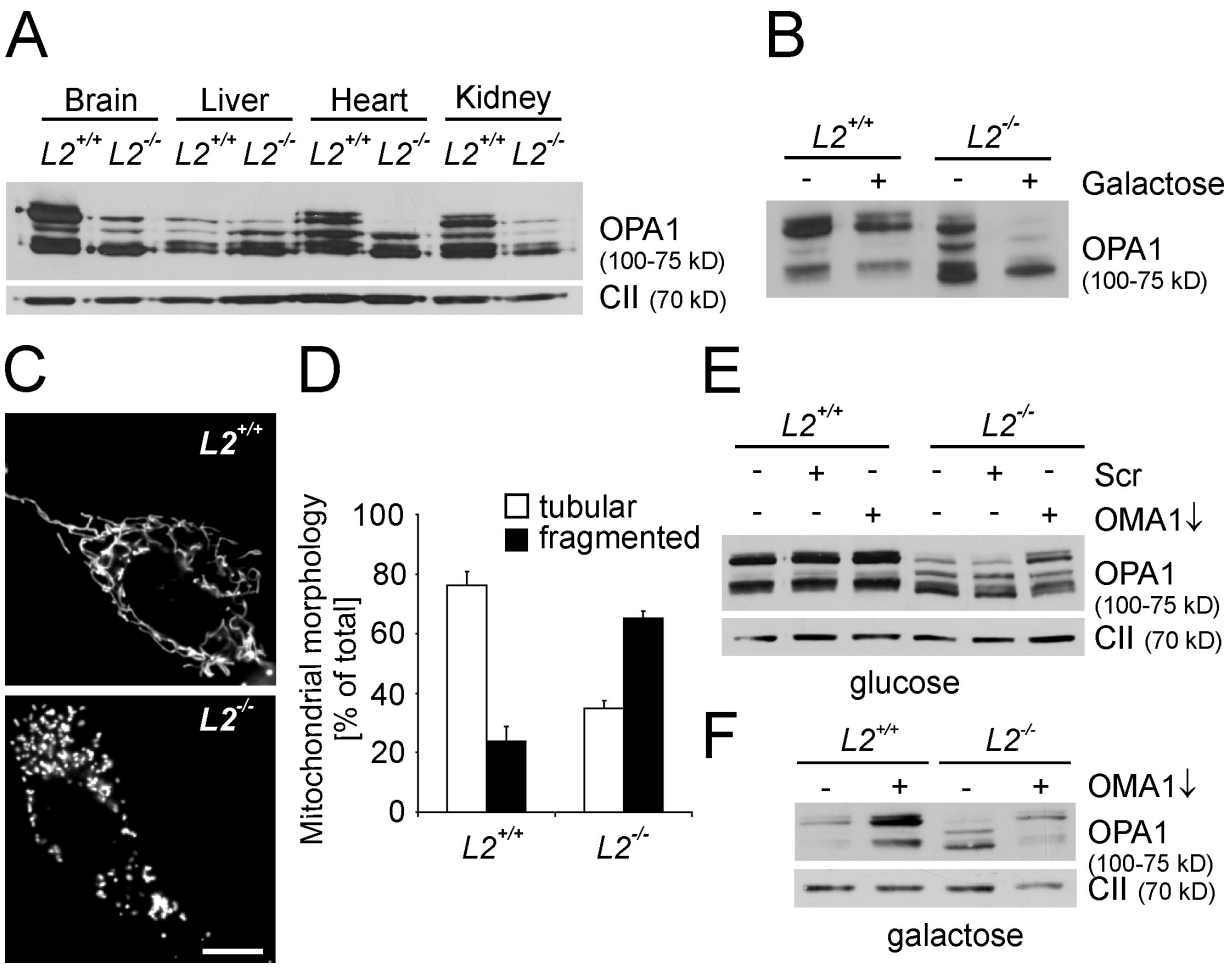

Figure 6. **Impaired OPA1 processing in *Afg3l2*$^{-/-}$ mice.** (A) Immunoblot analysis of mitochondria isolated from the brain, liver, heart, and kidney of WT (*L2*$^{+/+}$) or *Afg3l2*$^{-/-}$ (*L2*$^{-/-}$) mice using antisera directed against OPA1 and the 70-kD subunit of complex II (CII). (B) Immunoblot analysis of OPA1 in WT or *Afg3l2*$^{-/-}$ primary MEFs grown in the presence of glucose or galactose. (C and D) Mitochondrial morphology in WT or *Afg3l2*$^{-/-}$ cells was visualized by expression of a mitochondrially targeted GFP. >100 cells were scored. Bas represent means ± SD of three independent experiments. (E and F) Stabilization of long OPA1 isoforms in *Afg3l2*$^{-/-}$ MEFs grown in glucose or galactose upon down-regulation of OMA1. Immunoblot analysis was performed using specific antisera recognizing OPA1 and complex II. Scr, scrambled RNAi. Bar, 10 µm.

processing and mitochondrial morphology in *Afg3l2*$^{-/-}$ MEFs (Fig. 6, B–D). Deletion of *Afg3l2* only slightly affected cleavage of OPA1 in MEFs grown on glucose-containing medium, most likely because of the presence of AFG3L1 in these cells (Fig. 6 B). However, L-OPA1 was absent in *Afg3l2*$^{-/-}$ MEFs grown in the presence of galactose, i.e., conditions with an increased demand for mitochondrial respiratory function (Fig. 6 B). This was accompanied by a fragmentation of the mitochondrial network in the majority of these cells (Fig. 6, C and D). Depletion of OMA1 in immortalized *Afg3l2*$^{-/-}$ MEFs, cultured either in glucose- or galactose-containing medium, stabilized L-OPA1, providing further evidence that OMA1 mediates OPA1 processing if the function of the *m*-AAA protease is impaired (Fig. 6 E).

Mitochondrial dysfunction induces OPA1 processing by OMA1

We next examined whether OMA1 also cleaves OPA1 under other cellular conditions known to induce OPA1 processing. Current models suggest that a dysfunction of mitochondria accompanied by decreased mitochondrial ATP levels stimulates OPA1 processing and results in mitochondrial fragmentation (Duvezin-Caubet et al., 2006; Baricault et al., 2007). Therefore, we compared the accumulation of OPA1 isoforms in a human osteosarcoma cell line containing (WT) or lacking mitochondrial DNA (mtDNA; ρ^0; Fig. 7 A). Although long and short OPA1 isoforms accumulated in these cells in the presence of mtDNA, short isoforms accumulated in ρ^0 cells (Fig. 7 A). Strikingly, long OPA1 isoforms were detected after RNAi-mediated down-regulation of OMA1, suggesting that the loss of mtDNA induces OPA1 cleavage by OMA1.

OPA1 is converted into short isoforms upon dissipation of $\Delta\psi_m$ with the uncoupler CCCP or upon inhibition of the F_1F_O-ATP synthase with oligomycin (Fig. 7, B and C; Duvezin-Caubet et al., 2006; Ishihara et al., 2006). Down-regulation of OMA1 before the addition of CCCP or oligomycin significantly stabilized long OPA1 isoforms, indicating that OPA1 processing is mediated by OMA1 under both conditions (Fig. 7, B and C). In conclusion, these experiments identify OMA1 as the protease responsible for the inducible cleavage of OPA1 at processing site S1.

Downloaded from http://rupress.org/jcb/article-pdf/187/7/1023/1893434/jcb_200906084.pdf by guest on 23 April 2024

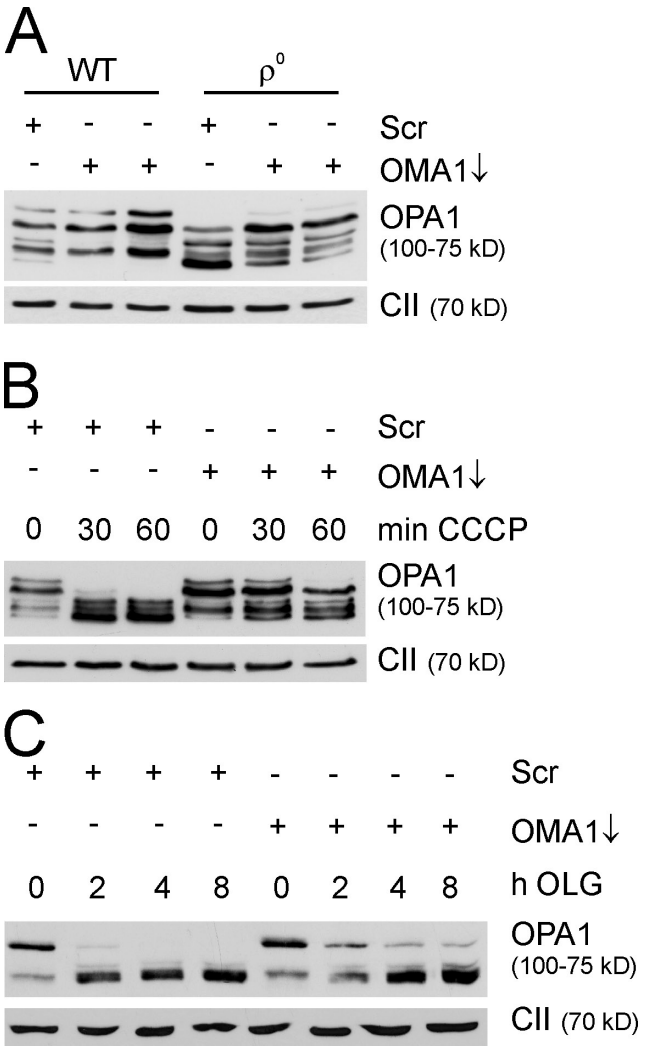

Figure 7. **Mitochondrial dysfunction induces OPA1 processing by OMA1.** (A) OMA1 stabilizes long OPA1 isoforms in the absence of mtDNA. Immunoblot analysis of human osteosarcoma cells (143B) using specific antisera recognizing OPA1 and the 70-kD subunit of complex II (CII). Cells lacking mtDNA (ρ^0) were transfected with OMA1-specific or scrambled (Scr) siRNA and compared with parental cells containing mtDNA (WT). Cell lysates were analyzed 72 h after transfection. (B and C) Stabilization of long OPA1 isoforms against CCCP (B)- and oligomycin (OLG; C)-induced processing in OMA1-depleted MEFs. MEFs transfected with OMA1-specific or scrambled siRNA were incubated after 48 h with 20 µM CCCP or after 60 h with 2 µM oligomycin for the indicated time periods. Cell lysates were analyzed by SDS-PAGE and immunoblotted with antibodies directed against OPA1 and complex II.

Discussion

Mutations in *m*-AAA protease subunits cause neurodegeneration, but pathogenic mechanisms remain enigmatic. Our results identify the *m*-AAA protease as a novel regulator of mitochondrial membrane fusion and cristae morphology, suggesting that *m*-AAA protease–associated diseases may represent a group of neurological disorders caused by deficiencies in mitochondrial dynamics. Murine AFG3L1- and AFG3L2-containing *m*-AAA protease isoenzymes exert at least partially overlapping activities during membrane fusion. Therefore, the relative expression of AFG3L1 and -2 in different tissues will determine whether or not a functional impairment of one *m*-AAA protease subunit affects the morphology of the mitochondrial network. Notably, the *m*-AAA protease subunit predominantly expressed in the mouse brain is AFG3L2, whereas AFG3L1 is only present at lower levels (Koppen et al., 2007; Martinelli et al., 2009). This explains severe neurological defects (Maltecca et al., 2008) and cerebellar degeneration in mice with reduced levels of AFG3L2-containing *m*-AAA isoenzymes (Martinelli et al., 2009), which is reminiscent of patients with heterozygous mutations in human *AFG3L2* (Cagnoli et al. 2008. Annual meeting of the American Society of Human Genetics. Abstr. 1501; DiBella et al. 2008. Annual meeting of the American Society of Human Genetics. Abstr. 216).

Whereas mitochondrial fusion depends on the presence of either AFG3L1 or -2, the third *m*-AAA protease subunit paraplegin is not required to maintain a reticulated mitochondrial network. Deletion of *Spg7*-encoding paraplegin did not affect mitochondrial morphology in MEFs. Moreover, phenotypes observed upon down-regulation of AFG3L1 and -2 were not worsened in paraplegin-deficient cells. However, it should be noted that an efficient depletion of AFG3L1 and -2 inactivates paraplegin that only exists in heterooligomeric complexes with AFG3L1 and -2 (Koppen et al., 2007). Thus, it is conceivable that paraplegin-containing isoenzymes may control mitochondrial morphology in cells expressing limiting levels of AFG3L1 and -2. This may explain the cell type–specific axonal degeneration associated with mutations in paraplegin both in mouse and human (Casari et al., 1998; Ferreirinha et al., 2004).

The *m*-AAA protease controls mitochondrial fusion via OPA1 (Fig. 8). The loss of AFG3L2 in various tissues of the mouse, down-regulation of AFG3L1 and -2 in MEFs, or the expression of a dominant-negative AFG3L2 variant in human cells decreases OPA1 stability and results in an increased processing and turnover of long OPA1 isoforms. This causes fragmentation of the tubular mitochondrial network, which is at least partially restored upon expression of an OPA1 variant lacking the cleavage site S1. Thus, our experiments link, for the first time, the function of AFG3L1 and -2 to OPA1 in vivo.

Strikingly, inactivation or loss of the *m*-AAA protease does not result in the accumulation of long OPA1 isoforms, as predicted by experiments in yeast (Duvezin-Caubet et al., 2007), but decreases their stability. The accelerated cleavage of OPA1 in the absence of the *m*-AAA protease is mediated by OMA1, a new member of a conserved and widespread family of membrane-bound M48 metallopeptidases. We have previously identified yeast Oma1 in the mitochondrial inner membrane as a peptidase that can substitute for the function of the *m*-AAA protease during degradation of a misfolded membrane protein (Käser et al., 2003). Similarly, synthetic growth defects have been observed when mutations in the bacterial AAA protease FtsH were combined with mutations in HtpX, which is a distant homologue of OMA1, indicating overlapping proteolytic activities (Shimohata et al., 2002). In agreement with these findings, we demonstrate in this study that mammalian OMA1, similar to the *m*-AAA protease, can cleave OPA1. The substrate specificity of OMA1 is distinct from yeast Oma1, which cleaves neither OPA1 when expressed in yeast nor the yeast OPA1 homologue

Downloaded from http://rupress.org/jcb/article-pdf/187/7/1023/1893434/jcb_200906084.pdf by guest on 23 April 2024

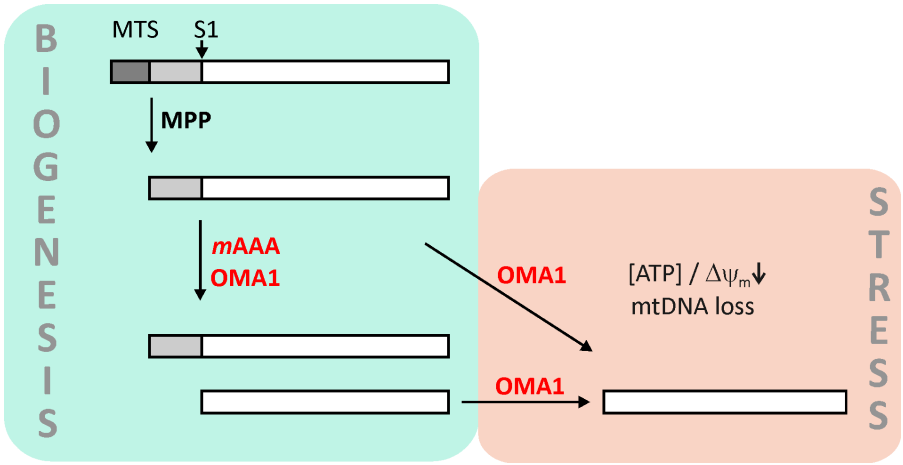

Figure 8. **Two peptidases regulate OPA1 cleavage at S1.** Newly imported OPA1 molecules are processed by the mitochondrial processing peptidase (MPP) in the matrix space (Ishihara et al., 2006). The stability of long OPA1 isoforms depends on *m*-AAA protease isoenzymes containing AFG3L1 and -2, which ensure the balanced formation of long and short OPA1 isoforms upon S1 cleavage and maintain mitochondrial fusion. The *m*-AAA protease itself may act as a processing peptidase for OPA1 or promote constitutive cleavage by OMA1. At decreased mitochondrial ATP levels, after dissipation of $\Delta\psi_m$, or in the absence of mtDNA, OMA1 promotes stress-induced OPA1 processing, resulting in the complete conversion of long OPA1 isoforms to short variants. Constitutive cleavage of OPA1 at site 2 is not depicted. MTS, mitochondrial targeting sequence.

Mgm1 (Duvezin-Caubet et al., 2007). Therefore, differences in substrate recognition by OMA1-like peptidases may explain why the loss of the *m*-AAA protease is not accompanied by increased OPA1 processing in yeast. Interestingly, mitochondrial rhomboid proteases, although highly conserved, also differ in their ability to cleave OPA1. Both yeast Pcp1 and its mammalian homologue PARL mediate processing of Mgm1, but neither of them cleave OPA1 when expressed in yeast (Duvezin-Caubet et al., 2007).

The regulation of OPA1 stability and processing at site S1 by two peptidases raises the question of which peptidase mediates constitutive and stress-induced OPA1 cleavage. Our experiments reveal that OMA1 promotes OPA1 processing if mitochondrial activities are impaired (Fig. 8). The loss of mtDNA, dissipation of $\Delta\psi_m$, or a decrease of mitochondrial ATP levels induces OPA1 processing by OMA1. The molecular mechanism of OMA1 activation under stress conditions remains to be determined. Mitochondrial dysfunction may alter the accessibility of the S1 cleavage site in OPA1, allowing stress-induced cleavage by OMA1. Alternatively, stress conditions may increase the proteolytic activity of OMA1 itself. It is also possible that stress conditions lower mitochondrial ATP levels and thereby *m*-AAA protease activity, resulting in the accumulation of an activator of OMA1.

In contrast to the stress-induced OPA1 cleavage, constitutive cleavage of OPA1 during mitochondrial biogenesis affects only a subset of the newly imported OPA1 molecules and results in an approximately equimolar accumulation of long and short isoforms. As both forms are required for mitochondrial fusion (Song et al., 2007), their balanced formation is critical for the maintenance of the mitochondrial network. Although our experiments identify OMA1 as the peptidase responsible for stress-induced OPA1 cleavage, two possibilities must be considered for constitutive OPA1 processing.

According to the first scenario, OMA1 is responsible for both constitutive and induced OPA1 cleavage. However, the *m*-AAA protease is required to stabilize long OPA1 isoforms and inhibit OMA1 activity under normal conditions, possibly exerting functions beyond a role as a processing enzyme. These may include the ATP-dependent membrane dislocation of OPA1 preceding its proteolytic cleavage. A similar nonproteolytic activity has been assigned to the *m*-AAA protease during the biogenesis of yeast cytochrome *c* peroxidase (Tatsuta et al., 2007). In yeast, the ATP-dependent mitochondrial import motor was proposed to regulate Mgm1 processing by the rhomboid protease in response to mitochondrial ATP levels in a process termed alternative topogenesis (Herlan et al., 2004). Constitutive OPA1 processing might be regulated in a similar manner. Notably, membrane dislocation could also be affected by an altered phospholipid composition of mitochondrial membranes, which has recently been observed in yeast mitochondria lacking the *m*-AAA protease (Osman et al., 2009). Several observations indeed suggest that OMA1 can cleave OPA1 in the presence of the *m*-AAA protease. Depletion of OMA1 in human osteosarcoma cells or in MEFs cultured in galactose-containing medium leads to the disappearance of OPA1 isoforms c and e, indicating that OMA1 can affect constitutive OPA1 processing at S1. Moreover, OMA1 is required for S1 cleavage of OPA1 overexpressed in MEFs. However, an OMA1-like peptidase appears to be absent in *Caenorhabditis elegans* and *Drosophila melanogaster*, although mitochondrial morphology depends on OPA1 in both organisms. In addition, neither down-regulation nor overexpression of OMA1 affects mitochondrial morphology in MEFs, suggesting that OMA1 is dispensable for the balanced formation of long and short OPA1 isoforms.

According to the second scenario, constitutive and stress-induced OPA1 processing are mediated by two distinct peptidases, which differ in their enzymatic properties: the ATP-dependent *m*-AAA protease ensures the balanced accumulation of long and short isoforms under constitutive conditions, whereas OMA1 acting in an ATP-independent manner completely converts long OPA1 isoforms into short forms under stress conditions. In agreement with a role of the *m*-AAA protease as a processing enzyme under normal conditions, reconstitution experiments in yeast demonstrate that AFG3L1 and -2 can cleave OPA1 in a heterologous environment (Duvezin-Caubet et al., 2007). Moreover, paraplegin binds OPA1 when overexpressed and stimulates OPA1 processing (Ishihara et al., 2006). OPA1 processing by ATP-dependent and -independent peptidases under different physiological conditions would resolve the apparent

Downloaded from http://rupress.org/jcb/article-pdf/187/7/1023/1893434/jcb_200906084.pdf by guest on 23 April 2024

caveat of previous studies suggesting that processing of OPA1 may involve the *m*-AAA protease but is accelerated at decreased mitochondrial ATP levels (Duvezin-Caubet et al., 2006, 2007; Ishihara et al., 2006; Baricault et al., 2007). It also offers an attractive possibility for regulation: low ATP levels may impair membrane dislocation of OPA1 possibly mediated by the *m*-AAA protease and thereby make OPA1 accessible for OMA1 cleavage under stress conditions. Clearly, further experiments are required to define the relative contribution of the *m*-AAA protease and OMA1 to constitutive OPA1 cleavage, which may also depend on relative expression levels in different tissues and cell types. Regardless, the identification of proteases involved in OPA1 processing now allows us to assess the relevance of an impaired OPA1 cleavage and mitochondrial fragmentation for the maintenance of cellular functions and for various disease states.

Materials and methods

Generation of immortalized MEFs lines

All animal procedures were performed according to protocols approved by the Institutional Animal Care and Use Committee. The generation of *Spg7*$^{-/-}$ mice (Ferreirinha et al., 2004) and *Afg3l2*$^{Emv66/Emv66}$ genetic characterization (Maltecca et al., 2008) were previously described. *Afg3l2*$^{Emv66/Emv66}$ mice were provided by G. Cox (The Jackson Laboratory, Bar Harbor, ME). Primary MEFs were established from embryonic day (E) 14.5 *Spg7*$^{-/-}$ or E13.5 *Afg3l2*$^{Emv66/Emv66}$ and littermate WT embryos and immortalized by SV40 transformation. MEFs were cultured in DME containing 4.5 g/liter glucose and supplemented with 10% FCS. When specified, MEFs were cultured in DME with 6 mM galactose. The human osteosarcoma-derived cell line 143B and its ρ^0 derivative were provided by R. Wiesner (University of Cologne, Cologne, Germany) and grown in medium supplemented with 50 µg/ml uridine.

Down-regulation of *m*-AAA protease subunits and OMA1

RNAi-mediated knockdown of paraplegin, AFG3L1 and -2, and OMA1 was performed using specific Stealth RNAi and the nontargeting Stealth RNAi negative control (Invitrogen). The sequences are 5′-GCGCGUCAUUGCUGGUACUGCUAAA-3′ for paraplegin, 5′-CCUGCCUCCGUACGCUCUAUCAAUA-3′ for AFG3L2, 5′-GCGAAACCAUGGUGGAGAAGCCAUA-3′ for AFG3L1, and 5′-GGAUACAGUCAAAGUUGCAGAGUA-3′, 5′-AGUUCUCAGAGAGUCUUCAUGGCUA-3′, and 5′-GCUUCUUGGUCUGAGUGCAUUUGGA-3′ for murine OMA1. For human OMA1, Stealth siRNAs with the sequences 5′-TGGACTACTGCTTGCTGCAAAGGCT-3′ and 5′-TGGCAGCAAATGGAGTTCGTTGATA-3′ were used. 10–20 nM of each siRNA was transfected twice with Lipofectamine (Invitrogen). Down-regulation was monitored by immunoblot analysis of cell lysates generated after 2 d if not indicated otherwise.

Expression of AFG3L2 variants and OMA1

Human *Afg3l2* was cloned into pcDNA5/FRT/TO, and mutations were introduced into the WB motif (E408Q) or the proteolytic center (E575Q). Stable transformants in FlpIn T-REx 293 cells were obtained by cotransfection with the plasmid pOG44, allowing expression of Flp-recombinase (Invitrogen). Expression of fusion proteins harboring a C-terminal hexahistidine epitope tag was induced with 1 µg/ml tetracycline. After 24 h, we analyzed cell lysates by immunoblotting and assessed mitochondrial morphology. The coding region of murine *Oma1* (GenBank/EMBL/DDBJ accession no. NM_025909) was cloned into the EcoRI–BamHI sites of the vector pEGFP-N2 in frame with GFP.

Assessment of cell growth

5×10^3 FlpIn T-REx 293 cells expressing AFG3L2 variants were seeded in medium with or without 1 µg/ml tetracycline. To assess the number of living cells in culture, we used the One Solution Cell Proliferation Assay (Promega) and monitored the conversion of a tetrazolium compound to formazan, determining the absorbance at 490 nm.

Fluorescence microscopy

Mitochondrial morphology was examined after expression of mito-DsRed using a microscope (DeltaVision; Applied Precision; Merkwirth et al., 2008). Fluorescence images were acquired using a camera (CoolSNAP HQ/ICX285; Sony) and a Plan-Apochromat N 60× NA 1.42 oil objective (Olympus). Image stacks were deconvoluted with the SoftWoRx Imaging Suite (Applied Precision). Image files were further processed with the CorelDRAW 11 Graphics Suite software (Corel). For colocalization of OMA1-GFP and mitochondria, we stained cells with MitoTracker red CMXRos (Invitrogen) and used a microscope (Eclipse E600; Nikon) and a Plan-Apochromat A 60× NA 1.40 oil objective (Nikon). Images were acquired with a confocal microscope (Radiance 2100; Bio-Rad Laboratories). For detection of the ER, cells were stained with an antiserum directed against calnexin and examined using an imaging station (Eclipse TE2000-S [Nikon] + CARV II [BD]) and a Plan-Apochromat VC 100× NA 1.40 oil objective (Nikon), and images acquired using a camera (QuantEM 512 SC; Photometrics) and deconvoluted with MetaMorph software (MDS Analytical Technologies).

Transmission electron microscopy

MEFs were plated on glass coverslips, transfected with siRNA, and after 48 h, flat embedded (Merkwirth et al., 2008). Ultrathin sections (60–70 nm) were cut and mounted on pioloform-coated copper grids (Plano). Sections were stained with lead citrate and uranyl acetate and viewed with a transmission electron microscope (JEM-2100; JEOL Ltd.) operated at 80 kV. Micrographs were taken using a charge-coupled device camera (Erlangshen ES500W; Gatan Inc.).

Polarographic measurements

Respiration of intact cells was measured at 37°C with a Clark-type electrode oxygraph (Hansatech Inc.). 2.5×10^6 cells were assayed in 250 mM saccharose, 20 mM Hepes, pH 7.4, 10 mM KH_2PO_4, 4 mM $MgCl_2$, 1 mM EDTA, 5 mM glucose, 2 mM pyruvate, and 4 mM glutamate. After recording endogenous respiration, ATP synthase was inhibited with 2 µM oligomycin followed by uncoupling of oxidative phosphorylation using CCCP with concentrations of 250–750 nM. Cellular respiration was inhibited with 2 mM KCN and was corrected to KCN-insensitive respiration.

Inhibitor experiments

To induce SIMH, MEFs were exposed to 1 µM CHX for 3 h 2–3 d after transfection with siRNAs and plasmids and were incubated for 5 h with the following protease inhibitors: 5 µM MG132, 0.5 mM *o*-phe, 50 µM pepstatin A, 0.5 mM Pefabloc SC, and 50 µM E-64d. To induce OPA1 cleavage, MEFs were treated either with 2 µM oligomycin 60 h after transfection or with 20 µM CCCP 48 h after transfection.

Antibodies

Polyclonal antibodies directed against murine *m*-AAA protease subunits were described previously (Koppen et al., 2007). An antiserum recognizing murine LON was provided by C. Suzuki (University of Medicine and Dentistry of New Jersey, Newark, NJ). The following commercially available antibodies were used: α-OPA1 (Invitrogen), α-Flag M2 (Sigma-Aldrich), α–SLP-2 (GenWay Biotech Inc.), α-calnexin (Stressgen), and α–complex II (Invitrogen).

Online supplemental material

Fig. S1 shows the mitochondrial morphology in paraplegin-deficient MEFs. Fig. S2 demonstrates the maintenance of the mitochondrial membrane potential in *Afg3l2*$^{-/-}$ mitochondria using TMRE fluorescence. Fig. S3 shows the stability of OPA1 in AFG3L1/AFG3L2-deficient cells lacking various mitochondrial proteases and the effect of an inhibition of cytosolic protein synthesis on OPA1 isoforms accumulating in *m*-AAA protease–deficient MEFs in the presence of MG132. Fig. S4 shows the quantification of OMA1 mRNA levels in MEFs after down-regulation of OMA1 by RNAi, demonstrates the assembly of AFG3L2 and -1 in *m*-AAA protease complexes in OMA1-deficient mitochondria by blue-native–PAGE analysis, and reveals normal processing of OMA1 in *m*-AAA protease–deficient mitochondria. Fig. S5 shows the accumulation of AFG3L1 and -2 in OMA1-deficient MEFs. Online supplemental material is available at http://www.jcb.org/cgi/content/full/jcb.200906084/DC1.

We thank Dr. G. Cox for providing the *Afg3l2*^{Emv66} mouse line, Dr. K. Mihara for OPA1 expression plasmids, Drs. J. Downward, B. de Strooper, and R. Wiesner for cell lines, Dr. C. Suzuki for LON-specific antibodies, and Dr. T. Tatsuta for discussion.

This work was supported by grants from the Deutsche Forschungsgemeinschaft, the German-Israeli-Project (DIP grant F.5.1), and the European Research Council to T. Langer and the Muscular Dystrophy Association, United Mitochondrial Disease Foundation, and Fondazione Cariplo to E.I. Rugarli.

Downloaded from http://rupress.org/jcb/article-pdf/187/7/1023/1893434/jcb_200906084.pdf by guest on 23 April 2024

Submitted: 15 June 2009
Accepted: 20 November 2009

References

Akepati, V.R., E.C. Müller, A. Otto, H.M. Strauss, M. Portwich, and C. Alexander. 2008. Characterization of OPA1 isoforms isolated from mouse tissues. *J. Neurochem.* 106:372–383. doi:10.1111/j.1471-4159.2008.05401.x

Amati-Bonneau, P., D. Milea, D. Bonneau, A. Chevrollier, M. Ferré, V. Guillet, N. Gueguen, D. Loiseau, M.A. de Crescenzo, C. Verny, et al. 2009. OPA1-associated disorders: phenotypes and pathophysiology. *Int. J. Biochem. Cell Biol.* 41:1855–1865. doi:10.1016/j.biocel.2009.04.012

Augustin, S., F. Gerdes, S. Lee, F.T. Tsai, T. Langer, and T. Tatsuta. 2009. An intersubunit signaling network coordinates ATP hydrolysis by m-AAA proteases. *Mol. Cell*. 35:574–585. doi:10.1016/j.molcel.2009.07.018

Bao, Y.C., H. Tsuruga, M. Hirai, K. Yasuda, N. Yokoi, T. Kitamura, and H. Kumagai. 2003. Identification of a human cDNA sequence which encodes a novel membrane-associated protein containing a zinc metalloprotease motif. *DNA Res.* 10:123–128. doi:10.1093/dnares/10.3.123

Baricault, L., B. Ségui, L. Guégand, A. Olichon, A. Valette, F. Larminat, and G. Lenaers. 2007. OPA1 cleavage depends on decreased mitochondrial ATP level and bivalent metals. *Exp. Cell Res.* 313:3800–3808. doi:10.1016/j.yexcr.2007.08.008

Casari, G., M. De Fusco, S. Ciarmatori, M. Zeviani, M. Mora, P. Fernandez, G. De Michele, A. Filla, S. Cocozza, R. Marconi, et al. 1998. Spastic paraplegia and OXPHOS impairment caused by mutations in paraplegin, a nuclear-encoded mitochondrial metalloprotease. *Cell*. 93:973–983. doi:10.1016/S0092-8674(00)81203-9

Cerveny, K.L., Y. Tamura, Z. Zhang, R.E. Jensen, and H. Sesaki. 2007. Regulation of mitochondrial fusion and division. *Trends Cell Biol.* 17:563–569. doi:10.1016/j.tcb.2007.08.006

Cipolat, S., T. Rudka, D. Hartmann, V. Costa, L. Serneels, K. Craessaerts, K. Metzger, C. Frezza, W. Annaert, L. D'Adamio, et al. 2006. Mitochondrial rhomboid PARL regulates cytochrome c release during apoptosis via OPA1-dependent cristae remodeling. *Cell*. 126:163–175. doi:10.1016/j.cell.2006.06.021

Dalal, S., M.F. Rosser, D.M. Cyr, and P.I. Hanson. 2004. Distinct roles for the AAA ATPases NSF and p97 in the secretory pathway. *Mol. Biol. Cell.* 15:637–648. doi:10.1091/mbc.E03-02-0097

Delettre, C., J.M. Griffoin, J. Kaplan, H. Dollfus, B. Lorenz, L. Faivre, G. Lenaers, P. Belenguer, and C.P. Hamel. 2001. Mutation spectrum and splicing variants in the *OPA1* gene. *Hum. Genet.* 109:584–591. doi:10.1007/s00439-001-0633-y

Duvezin-Caubet, S., R. Jagasia, J. Wagener, S. Hofmann, A. Trifunovic, A. Hansson, A. Chomyn, M.F. Bauer, G. Attardi, N.G. Larsson, et al. 2006. Proteolytic processing of OPA1 links mitochondrial dysfunction to alterations in mitochondrial morphology. *J. Biol. Chem.* 281:37972–37979. doi:10.1074/jbc.M606059200

Duvezin-Caubet, S., M. Koppen, J. Wagener, M. Zick, L. Israel, A. Bernacchia, R. Jagasia, E.I. Rugarli, A. Imhof, W. Neupert, et al. 2007. OPA1 processing reconstituted in yeast depends on the subunit composition of the *m*-AAA protease in mitochondria. *Mol. Biol. Cell*. 18:3582–3590. doi:10.1091/mbc.E07-02-0164

Ferreirinha, F., A. Quattrini, M. Pirozzi, V. Valsecchi, G. Dina, V. Broccoli, A. Auricchio, F. Piemonte, G. Tozzi, L. Gaeta, et al. 2004. Axonal degeneration in paraplegin-deficient mice is associated with abnormal mitochondria and impairment of axonal transport. *J. Clin. Invest.* 113:231–242.

Frezza, C., S. Cipolat, O. Martins de Brito, M. Micaroni, G.V. Beznoussenko, T. Rudka, D. Bartoli, R.S. Polishuck, N.N. Danial, B. De Strooper, and L. Scorrano. 2006. OPA1 controls apoptotic cristae remodeling independently from mitochondrial fusion. *Cell*. 126:177–189. doi:10.1016/j.cell.2006.06.025

Griparic, L., N.N. van der Wel, I.J. Orozco, P.J. Peters, and A.M. van der Bliek. 2004. Loss of the intermembrane space protein Mgm1/OPA1 induces swelling and localized constrictions along the lengths of mitochondria. *J. Biol. Chem.* 279:18792–18798. doi:10.1074/jbc.M400920200

Griparic, L., T. Kanazawa, and A.M. van der Bliek. 2007. Regulation of the mitochondrial dynamin-like protein Opa1 by proteolytic cleavage. *J. Cell Biol.* 178:757–764. doi:10.1083/jcb.200704112

Herlan, M., C. Bornhövd, K. Hell, W. Neupert, and A.S. Reichert. 2004. Alternative topogenesis of Mgm1 and mitochondrial morphology depend on ATP and a functional import motor. *J. Cell Biol.* 165:167–173. doi:10.1083/jcb.200403022

Hoppins, S., L. Lackner, and J. Nunnari. 2007. The machines that divide and fuse mitochondria. *Annu. Rev. Biochem.* 76:751–780. doi:10.1146/annurev.biochem.76.071905.090048

Ishihara, N., Y. Fujita, T. Oka, and K. Mihara. 2006. Regulation of mitochondrial morphology through proteolytic cleavage of OPA1. *EMBO J.* 25:2966–2977. doi:10.1038/sj.emboj.7601184

James, D.I., P.A. Parone, Y. Mattenberger, and J.C. Martinou. 2003. hFis1, a novel component of the mammalian mitochondrial fission machinery. *J. Biol. Chem.* 278:36373–36379. doi:10.1074/jbc.M303758200

Käser, M., M. Kambacheld, B. Kisters-Woike, and T. Langer. 2003. Oma1, a novel membrane-bound metallopeptidase in mitochondria with activities overlapping with the *m*-AAA protease. *J. Biol. Chem.* 278:46414–46423. doi:10.1074/jbc.M305584200

Koppen, M., M.D. Metodiev, G. Casari, E.I. Rugarli, and T. Langer. 2007. Variable and tissue-specific subunit composition of mitochondrial *m*-AAA protease complexes linked to hereditary spastic paraplegia. *Mol. Cell. Biol.* 27:758–767. doi:10.1128/MCB.01470-06

Koppen, M., F. Bonn, S. Ehses, and T. Langer. 2009. Autocatalytic processing of *m*-AAA protease subunits in mitochondria. *Mol. Biol. Cell*. 20:4216–4224. doi:10.1091/mbc.E09-03-0218

Kremmidiotis, G., A.E. Gardner, C. Settasatian, A. Savoia, G.R. Sutherland, and D.F. Callen. 2001. Molecular and functional analyses of the human and mouse genes encoding AFG3L1, a mitochondrial metalloprotease homologous to the human spastic paraplegia protein. *Genomics*. 76:58–65. doi:10.1006/geno.2001.6560

Lenaers, G., P. Reynier, G. Elachouri, C. Soukkarieh, A. Olichon, P. Belenguer, L. Baricault, B. Ducommun, C. Hamel, and C. Delettre. 2009. OPA1 functions in mitochondria and dysfunctions in optic nerve. *Int. J. Biochem. Cell Biol.* 41:1866–1874. doi:10.1016/j.biocel.2009.04.013

Maltecca, F., A. Aghaie, D.G. Schroeder, L. Cassina, B.A. Taylor, S.J. Phillips, M. Malaguti, S. Previtali, J.L. Guénet, A. Quattrini, et al. 2008. The mitochondrial protease AFG3L2 is essential for axonal development. *J. Neurosci.* 28:2827–2836. doi:10.1523/JNEUROSCI.4677-07.2008

Martinelli, P., V. La Mattina, A. Bernacchia, R. Magnoni, F. Cerri, G. Cox, A. Quattrini, G. Casari, and E.I. Rugarli. 2009. Genetic interaction between the *m*-AAA protease isoenzymes reveals novel roles in cerebellar degeneration. *Hum. Mol. Genet.* 18:2001–2013. doi:10.1093/hmg/ddp124

Meeusen, S., R. DeVay, J. Block, A. Cassidy-Stone, S. Wayson, J.M. McCaffery, and J. Nunnari. 2006. Mitochondrial inner-membrane fusion and crista maintenance requires the dynamin-related GTPase Mgm1. *Cell*. 127:383–395. doi:10.1016/j.cell.2006.09.021

Merkwirth, C., S. Dargazanli, T. Tatsuta, S. Geimer, B. Löwer, F.T. Wunderlich, J.C. von Kleist-Retzow, A. Waisman, B. Westermann, and T. Langer. 2008. Prohibitins control cell proliferation and apoptosis by regulating OPA1-dependent cristae morphogenesis in mitochondria. *Genes Dev.* 22:476–488. doi:10.1101/gad.460708

Olichon, A., L. Baricault, N. Gas, E. Guillou, A. Valette, P. Belenguer, and G. Lenaers. 2003. Loss of OPA1 perturbates the mitochondrial inner membrane structure and integrity, leading to cytochrome *c* release and apoptosis. *J. Biol. Chem.* 278:7743–7746. doi:10.1074/jbc.C200677200

Osman, C., M. Haag, C. Potting, J. Rodenfels, P.V. Dip, F.T. Wieland, B. Brügger, B. Westermann, and T. Langer. 2009. The genetic interactome of prohibitins: coordinated control of cardiolipin and phosphatidylethanolamine by conserved regulators in mitochondria. *J. Cell Biol.* 184:583–596. doi:10.1083/jcb.200810189

Shimohata, N., S. Chiba, N. Saikawa, K. Ito, and Y. Akiyama. 2002. The Cpx stress response system of *Escherichia coli* senses plasma membrane proteins and controls HtpX, a membrane protease with a cytosolic active site. *Genes Cells*. 7:653–662. doi:10.1046/j.1365-2443.2002.00554.x

Smirnova, E., D.L. Shurland, S.N. Ryazantsev, and A.M. van der Bliek. 1998. A human dynamin-related protein controls the distribution of mitochondria. *J. Cell Biol.* 143:351–358. doi:10.1083/jcb.143.2.351

Song, Z., H. Chen, M. Fiket, C. Alexander, and D.C. Chan. 2007. OPA1 processing controls mitochondrial fusion and is regulated by mRNA splicing, membrane potential, and Yme1L. *J. Cell Biol.* 178:749–755. doi:10.1083/jcb.200704110

Tatsuta, T., S. Augustin, M. Nolden, B. Friedrichs, and T. Langer. 2007. *m*-AAA protease-driven membrane dislocation allows intramembrane cleavage by rhomboid in mitochondria. *EMBO J.* 26:325–335. doi:10.1038/sj.emboj.7601514

Tondera, D., S. Grandemange, A. Jourdain, M. Karbowski, Y. Mattenberger, S. Herzig, S. Da Cruz, P. Clerc, I. Raschke, C. Merkwirth, et al. 2009. SLP-2 is required for stress-induced mitochondrial hyperfusion. *EMBO J.* 28:1589–1600. doi:10.1038/emboj.2009.89

Weibezahn, J., C. Schlieker, B. Bukau, and A. Mogk. 2003. Characterization of a trap mutant of the AAA+ chaperone ClpB. *J. Biol. Chem.* 278:32608–32617. doi:10.1074/jbc.M303653200

Westermann, B. 2008. Molecular machinery of mitochondrial fusion and fission. *J. Biol. Chem.* 283:13501–13505. doi:10.1074/jbc.R800011200

Downloaded from http://rupress.org/jcb/article-pdf/187/7/1023/1893434/jcb_200906084.pdf by guest on 23 April 2024